ELSEVIER

Journal of Power Sources 99 (2001) 70–77

JOURNAL OF POWER SOURCES

www.elsevier.com/locate/jpowsour

Thermal behavior analysis of lithium-ion batteries for electric and hybrid vehicles

Noboru Sato*

Honda R&D Co., Ltd., Tochigi R&D Center, 4630 Shimotakanezawa, Haga-machi, Haga-gun, Tochigi 321-3393, Japan

Received 4 September 2000; received in revised form 8 November 2000; accepted 20 December 2000

Abstract

Thermodynamics experiment and study were carried out for the lithium-ion (Li-ion) batteries that are expected as the power sources for electric and hybrid vehicles. It is confirmed that the heat coming in and going out depend on charging and discharging, respectively. And the thermal generation factors will be decomposed to three elements: reaction heat value Q_r, polarization heat value Q_p, and Joule heat value Q_J. Furthermore, the contribution degree of each factor was able to be expressed quantitatively by dividing these thermal generation factors for charging and discharging.

The accuracy of thermodynamics logic was verified since the thermodynamics calculation coincided with the experimental data of thermal generation for the practical Li-ion batteries for electric vehicles (EV). It is possible to utilize the calculation and simulation for the development of Li-ion battery and the establishment of thermal control technology not only for EV but also for hybrid electric vehicles (HEV).

Keywords: Lithium-ion battery; Thermal behavior; Thermodynamics; Electric and hybrid vehicle; Entropy; Heat element

1. Introduction

The active development of electric vehicles (EV), hybrid electric vehicles (HEV), and fuel cell vehicles (FCV) has been accompanied by leaps in battery technology as applied to energy storage. Particularly high expectations are being placed on advances in high-performance nickel-metal hydride (Ni–MH) batteries and Li-ion batteries. Ni–MH batteries offer superior performance, reliability, and safety, and are already on the market in the Honda EV Plus released 4 years ago and the HEV Insight released 1 year ago.

Heat control is an important issue in Ni–MH, Li-ion, and other batteries, which are susceptible to the effects of heat. Temperatures above 50°C will lower the charging efficiency or lower the longevity properties of these batteries. Thermal management must also take battery reactions and thermal generation factors into account, as exothermic behavior can vary greatly depending on the battery system.

However, there are almost no papers that discuss the thermal behavior of batteries from a thermodynamic perspective [1,2]. Only one existing report quantitatively analyzes the thermal behavior of Ni–MH batteries [3]. Working from this report, the author focuses on Li-ion batteries, which are expected to have expanded application in the future, with the goal of clarifying the exothermic mechanism through analysis of thermal generation factors, and determining the proper approach to thermal management for Li-ion batteries.

2. The operating principle and characteristics of Li-ion batteries

A Li-ion battery generally comprises a positive electrode of lithium cobalt oxide ($LiCoO_2$), lithium manganese oxide ($LiMnO_2$ or $LiMn_2O_4$), or lithium nickel oxide ($LiNiO_2$), or a hybrid material comprised thereof, a negative electrode of hard carbon or graphite, an electrolyte of a non-aqueous solvent comprising ethylene carbonate (EC) or propylene carbonate, and $LiPF_6$ as a supporting electrolyte. These charging reactions of this battery type are expressed with Eqs. (1)–(3) below.

$$\text{Positive electrode}: \quad LiCoO_2 \rightarrow Li_{1-x}CoO_2 + xLi^+ + xe \tag{1}$$

$$\text{Negative electrode}: \quad C + xLi^+ + xe \rightarrow CLi_x \tag{2}$$

$$\text{Whole reaction}: \quad LiCoO_2 + C \rightarrow Li_{1-x}CoO_2 + CLi_x \tag{3}$$

* Fax: +81-28-677-6790.

0378-7753/01/$ – see front matter
PII: S0378-7753(01)00478-5

Nomenclature

A	frequency factor
C	battery heat capacity
E_a	activation energy
E_e	battery's electromotive force
F	Faraday constant
ΔG	change in Gibbs's free energy
ΔH	enthalpy change of the battery reaction
I_c	battery charge current
I_d	battery discharge current
K	electrode degradable reaction rate
Q	quantity of heat
Q_c	charge heat
Q_d	discharge heat
Q_J	Joule heat
Q_p	polarization heat
Q_r	reaction heat
Q_s	side reaction heat
Q_t	total battery heat
R	gas constant
R_e	electrical resistance
R_p	polarization resistance
R_{pc}	polarization resistance during charge
R_{pd}	polarization resistance during discharge
R_t	battery total resistance
R_{tc}	battery resistance during charge
R_{td}	battery resistance during discharge
ΔS	entropy change
T	absolute temperature
T_r	thermal radiation temperature
W	battery output

In short, these are solid-state reactions in an intercalation mechanism in which (Fig. 1) the negative electrode occludes lithium ions during charging, while the positive electrode occludes lithium ions during discharging.

The use of electrode active materials that are lighter than those in lead-acid batteries or Ni–MH batteries results in the characteristically large energy density per weight of Li-ion batteries. This, combined with their large volume energy density, is why Li-ion batteries have replaced Ni–MH batteries in almost all computers and mobile phone applications. The next logical step is to develop technology for large Li-ion batteries, with the development of such batteries for EVs and HEVs is gaining momentum.

3. Impact of the thermal action of Li-ion batteries

The performance of nearly all types of secondary batteries is normally degraded by the thermal action. At low temperatures, output falls primarily because of the electrolyte's decrease in electric conductivity, while high temperatures often lower the battery's longevity. As an example, data from the heat-induced capacity degradation of a Li-ion battery for a 1.25 Ah of Sony 18650 cylindrical type appliance are given.

The experiment conditions were defined as an ambient temperature of 25°C, 2.5 h total of charge time at a 1 A constant current and a 4.2 V constant voltage, discharging at a constant current of 1, 2, 3, and 4 A, and a final voltage of 2.5 V. There was 10 min rest time after charging and discharging, and the entire process from charge to discharge was defined as one cycle. Fig. 2 gives the relationship between cycle count and capacity ratio at each current value in this experiment. Fig. 3 shows the relationship between current value and average battery temperature during discharge.

Because of the safety issues that still preclude experimentation that would intentionally induce temperature increases in a large-sized Li-ion battery for electric and hybrid vehicle application, data from appliance batteries were used instead. However, exothermic mechanisms and effects are essentially the same.

In Fig. 3, the lower battery temperature during 4 A discharge than at 3 A discharge is caused by the shorter discharge time at 4 A. Therefore, the minimum voltage of 2.5 V was reached and the next cycle was begun before the

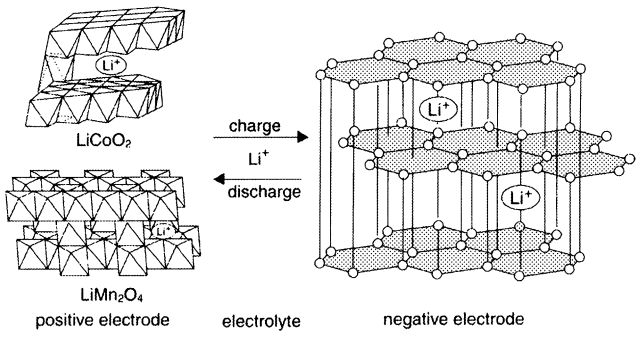

Fig. 1. Crystal structures of lithium cobalt oxide and lithium manganese oxide as the positive active material and carbon material as the negative material.

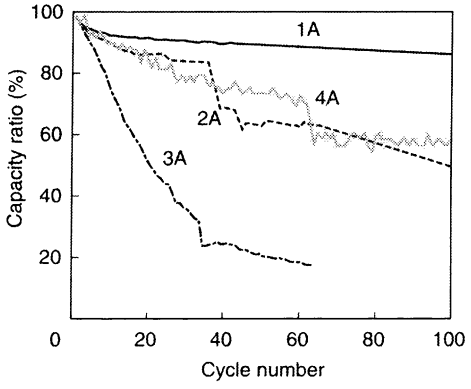

Fig. 2. Change of the capacity ratio for each discharge current for Sony 18650 cylindrical Li-ion batteries.

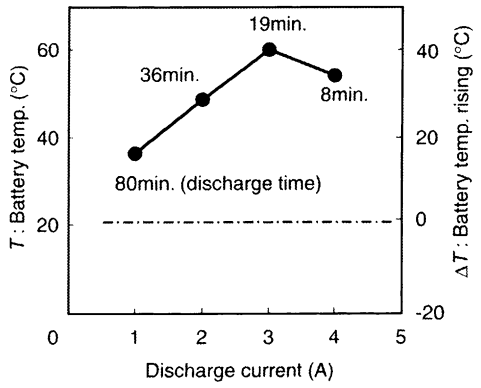

Fig. 3. Relationship between the discharge current and the battery temperature rising.

battery temperature could rise keeping battery temperature relatively low.

Let us next consider degradable rate. The primary causes of degradation are most likely electrode bulk degradation, growth of electrode surface film and changes in composition, and the accompanying electrolyte decomposition. As Eqs. (4)–(12) show, degradation progresses due to the complex interaction of multiple reactions [4–10]. However, the quantitative degradation mechanism has not yet been clarified.

$$HCOOCH_3 \rightarrow HCOOLi + \text{alkanes} \quad (4)$$

$$HCOOCH_3 \rightarrow CH_3COLi + CO_2 + H_2 \quad (5)$$

$$EC \rightarrow (CH_2OCO_2Li)_2 + CH_2{=}CH_2 \quad (6)$$

$$ROCO_2Li + H_2O \rightarrow ROH + CO_2 + Li_2CO_3 \quad (7)$$

$$H_2O \rightarrow LiOH + H_2 \rightarrow Li_2O + H_2 \quad (8)$$

$$HCOOCH_3 + LiOH \rightarrow HCOOLi + CH_3OH \quad (9)$$

$$CH_3OH \rightarrow CH_3OLi + H_2 \quad (10)$$

$$LiPF_6 \rightarrow 3LiF + PF_3 \quad (11)$$

$$PF_3 \rightarrow Li_xPF_y + LiF \quad (12)$$

At the same time, the electrode degradable reaction rate can be expressed with Eq. (13) for any degradation mechanism as above.

$$K = \frac{I}{nF} \quad (13)$$

where K is the electrode degradable reaction rate (mol/s), I the current value consumed by degradation (A), n the reaction order, F the Faraday constant (9.64846×10^4 C/equiv.). To calculate the electrode degradable reaction rate using Eq. (13), capacity at the point where initial capacity has dropped by 20% (this point is defined as cycle life) is divided by the total amount of time elapsed throughout the cycle life, thus arriving at the current value that is consumed by battery degradation. As reaction order (n) is either 1 or 2, as in Eqs. (4)–(12), Eq. (13) is used to calculate the degradable reaction rate at each temperature for each reaction order. The results are in Table 1.

Defining activation energy as E_a (kJ/mol), gas constant as R (8.31451 J/K mol), and frequency factor as A (A/mol s), Arrhenius equation can be expressed as in Eq. (14).

$$\ln K = \frac{-E_a}{RT} + \ln A \quad (14)$$

Eq. (14) can then be used to logarithmically convert degradable reaction rate K from the inverse of battery absolute temperature. These results are plotted in Fig. 4. This approximation equation verifies that correlation coefficient R is 0.987, suggesting good correlation. Thus, the mechanism by which degradation is effected by temperature change can be approximated using degradable reaction rate K.

Eq. (14) yields the following values: $E_a = 150.6$ kJ/mol, $A_{n=1} = 3.643$ mol/s, $A_{n=2} = 3.500$ mol/s. Here, activation energy refers to E_a in Fig. 5, and is the potential energy barrier that must normally be overcome for the reaction to proceed. In other words, it is the energy needed for the degradation reaction to occur in the Li-ion battery.

At low temperatures, the electrode surface in a Li-ion battery is relatively stable, as indicated by the energy level in Fig. 5 (the broken line). At higher temperatures, however, the potential energy level rises to the energy level indicated by the solid line. In this state, the smaller difference relative to the potential energy in the activated state makes it easier for the peak in the illustration to be exceeded, at which point the degradable reaction rate speeds up.

Reaction energy when $n = 1$ is roughly the same as when $n = 2$, but frequency factor A exhibits different values. This represents the differing frequency of the various reactions in Eqs. (4)–(12), and is also seen as a result of complex degradation reactions.

The preceding shows how battery temperature is a major determinant of degradation. Next is an in-depth analysis of the exothermic mechanism operating during charge and discharge of the battery.

Table 1
Degradable reaction rate

I (A)	1	2	3	4
ΔT (°C)	11.3	23.7	35.0	29.2
Cycle number (∞)	500	38	10	27
Degradable rate: $K_{n=1}$ (mol/s)	1.25E−09	1.99E−08	8.24E−08	3.23E−08
Degradable rate: $K_{n=2}$ (mol/s)	6.25E−10	9.93E−09	4.12E−08	1.61E−08

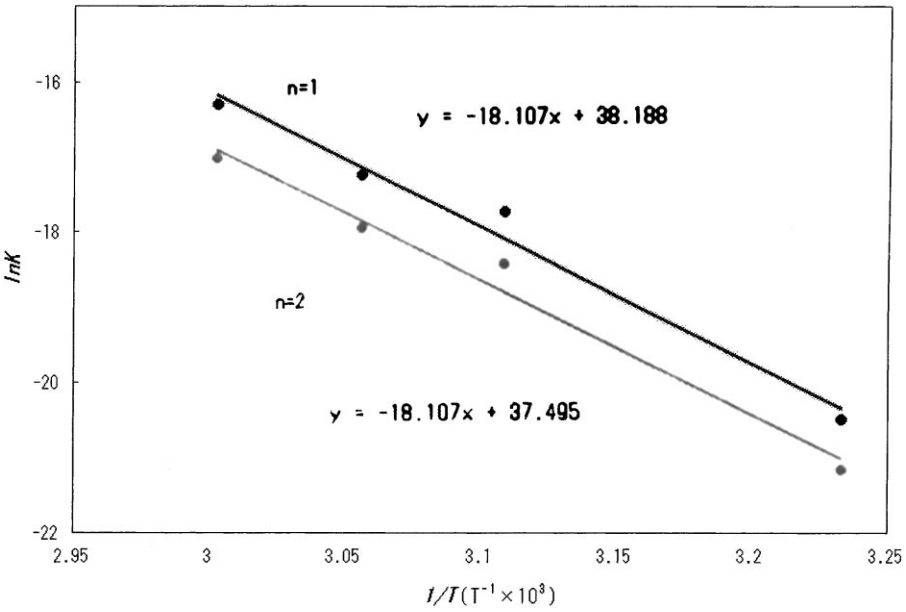

Fig. 4. Arrhenius plot for the practical Li-ion battery.

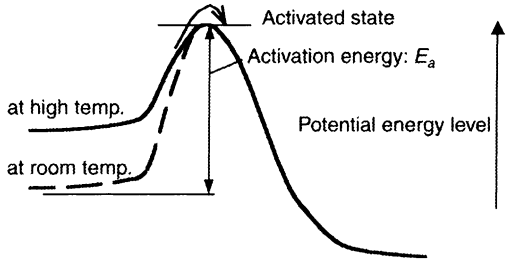

Fig. 5. Energy barrier for chemical reactions.

4. Analysis of the battery's exothermic mechanism

A battery generally releases and absorbs heat during charge and discharge reactions. Because a reversible battery maintains a thermodynamic relationship at a constant temperature and pressure, the release of heat in battery reactions can be expressed in terms of ΔG, the change in Gibbs's free energy equivalent to electric work, as in Eq. (15)

$$\Delta G = \Delta H - T\,\Delta S \tag{15}$$

where ΔH is the enthalpy change in battery reaction, T the absolute temperature, and ΔS the entropy change in battery reaction. If the battery reaction progresses in reverse, then the discharge and charge reactions are the reverse of one another, and so the intake and release of heat is reversed as well. $T\,\Delta S$ in Eq. (15) corresponds to thermal energy in the battery reaction, and is expressed as reaction heat value Q_r in Eq. (16).

$$Q_r = T\,\Delta S = T\left(-\frac{\delta \Delta G}{\delta T}\right) \tag{16}$$

On the other hand, as for ΔG, if Eq. (17) holds true when the battery's electromotive force is E_e, Faraday constant is F, and charge number involved in the battery reaction is n, Eq. (16) can be converted to Eq. (18).

$$\Delta G = -nFE_e \tag{17}$$

$$Q_r = nFT\left(\frac{\delta E_e}{\delta T}\right) \tag{18}$$

However, as the battery's actual terminal voltage (E_f) deviates from equilibrium electromotive force (i.e. electrode potential) due to electrochemical polarization of the battery, it is accompanied by heat generation Q_p, which is the energy loss due to this polarization. Q_p is heat generation during charge and discharge. The battery reaction also results in side reactions, self-discharge and such due to electrolyte decomposition, which are manifested as thermal factor Q_s. Also added is Joule heat Q_J, which is caused by the battery's electrical resistance component. Total heat generation in the battery reaction, Q_t, is therefore expressed with Eq. (19).

$$Q_t = Q_r + Q_p + Q_s + Q_J = nFT\left(\frac{\delta E_e}{\delta T}\right) + Q_p + Q_s + Q_J \tag{19}$$

5. Analysis of the thermal behavior of Li-ion batteries

5.1. Thermal behavior during charge and discharge

The side reaction accompanying electrolyte decomposition at the end of the charge period is an irreversible gas generation reaction, which results in the generation of flammable gas. This is an issue that necessitates control in the stage before this side reaction occurs. Therefore, unlike a Ni–MH battery, the term Q_s is necessarily zero.

In actuality, the side reaction that accompanies degradation most likely generates minute quantities of heat as stated in Section 3, but this amount is small enough to disregard in comparison to other quantities of heat.

During discharge, the battery heat reaction component (Q_r) is exothermic, and so heat stress caused by the battery reaction is greater than during charging. The addition of Joule heat Q_J resulting from the battery's electrical resistance component further increases heat generation during discharge. Although, this heat generation is too large to disregard in batteries having considerable self-discharge and such, the self-discharge of currently marketed Li-ion batteries is low enough to disregard for the purposes of analyzing thermal behavior, and so is not addressed here. Thus, the term Q_s is zero during discharge as well.

In short, in the case of a Li-ion battery, Eq. (19) can be replaced by Eq. (20) depending on use restrictions. It should be noted, however, that as stated above, the dominant thermal factors are different during charge and discharge.

$$Q_t = Q_r + Q_p + Q_J = nFT\left(\frac{\delta E_e}{\delta T}\right) + Q_p + Q_J \tag{20}$$

5.2. Analysis of thermal behavior factors

5.2.1. Reaction heat value: Q_r

The reaction heat during charge in a Li-ion battery corresponds to the heat absorbed when lithium ions from the positive electrode are intercalated by the negative electrode. In addition, a quantity of heat equivalent to this is generated during discharge. If total generated heat in Eqs. (1) and (2) is Q_1 (kJ/mol) and battery charge current is I_c, then the corresponding reaction heat value per unit time (Q_r) is as expressed in Eq. (21) for the charging process of Eq. (3). In this process, the exothermic reaction will not appear, but the endothermic reaction will be observed. Thus, reaction heat value per unit time is expressible with a first-order function of charge current.

$$Q_r = \frac{Q_1}{(F/3600)} I_c = -3.37 \times 10^{-2} Q_1 I_c \ \ (\mathrm{kJ/h}) \tag{21}$$

5.2.2. Polarization heat value: Q_p

The reason that polarization results in a discrepancy with theoretical electromotive force in an actual battery reaction is that energy is required for the diffusion and movement of atoms in the battery reaction process. Lithium ions have a low chemical diffusion coefficient of 5×10^{-9} cm^2/s [11], and so diffusion and movement inside the electrodes are the predominant factors. Also discussed in Section 3, the electrode surface degradation accompanying the cycle also increases polarization. Thus, the key to controlling heat generation is a structural design that reduces polarization.

R_{pd}, the polarization resistance component that accompanies this polarization during discharge is manifested as the polarization resistance component corresponding to a portion of total battery resistance during discharge (R_{td}), and so can be expressed as shown in Eq. (22), where R_e is the electrical resistance component. Polarization heat value per unit time (Q_{pd}) is expressed with Eq. (23), where I_d is the discharge current. In the case of charging, resistance component R_{pd} and current value I_d are replaced with R_{pc} and I_c, respectively, yielding Eqs. (24) and (25).

$$R_{pd} = R_{td} - R_e \tag{22}$$

$$Q_{pd} = I_d^2 R_{pd} \ \ (\mathrm{W}) = 3.60 I_d^2 R_{pd} \ \ (\mathrm{kJ/h}) \tag{23}$$

$$R_{pc} = R_{tc} - R_e \tag{24}$$

$$Q_{pc} = I_c^2 R_{pc} \ \ (\mathrm{W}) = 3.60 I_c^2 R_{pc} \ \ (\mathrm{kJ/h}) \tag{25}$$

Because this heat generation is manifested as total Joule heat, polarization heat values (Q_{pd} and Q_{pc}) are not calculated directly, but rather must be calculated by separating the polarization resistance components out of the total resistance components in Eqs. (22) and (24). And then they were calculated as the heat generation corresponding to that resistance component.

5.2.3. Joule heat of the electrical resistance component: Q_J

Heat generation that is dependent on the battery's internal resistance is manifested as Joule heat. However, as shown in Eqs. (22) and (24), internal resistance comprises electrical resistance and polarization-induced reaction resistance, with the heat generated being the total of the two. As for the latter, as stated in Section 5.2.2, Joule heat generated per unit time due to the electrical resistance portion is expressible with Eq. (26), where I_d is the discharge current. Joule heat during charging can be expressed with Eq. (27) by replacing I_d with I_c and electrical resistance R_{ed} with R_{ec}.

$$Q_J = I_d^2 R_{ed} \ \ (\mathrm{W}) = 3.60 I_d^2 R_{ed} \ \ (\mathrm{kJ/h}) \tag{26}$$

$$Q_J = I_c^2 R_{ec} \ \ (\mathrm{W}) = 3.60 I_c^2 R_{ec} \ \ (\mathrm{kJ/h}) \tag{27}$$

Thus, reducing this Joule heat necessitates a material design and a structural design that minimize the battery's electrical resistance component (R_e), which is determined by the current network linking the collector and the electrode active material by the separator (a nonconductive material) and the electrolyte among others. As Fig. 6 shows, R_{td} changes depending on the discharge condition (DOD), increasing in the zone where the DOD value is large. Here, 50% DOD is defined as the baseline value of 1.0.

As Fig. 7 shows, the PC/DMC/$LiPF_6$ electrolytes commonly used in Li-ion batteries have an electric conductivity that varies depending on temperature. A shift in battery temperature to the low-temperature side therefore increases the battery's internal resistance.

5.2.4. Heat balance during charge and discharge

5.2.4.1. Heat balance during charge. Based on the above and using Eq. (20), charge heat balance per unit time (Q_c) is

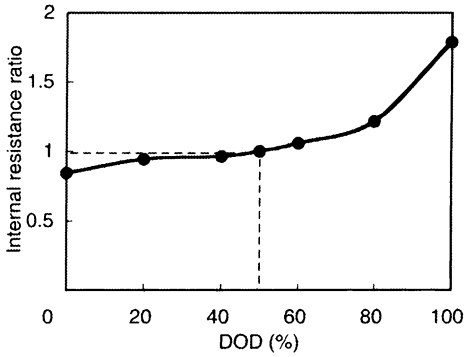

Fig. 6. Relationship between DOD and internal resistance ratio.

expressed with Eq. (28).

$$Q_c = Q_r + Q_{pc} + Q_J = -3.73 \times 10^{-2} Q_1 I_c + 3.60 I_c^2 R_{pc} + 3.60 I_c^2 R_{ec} = -3.73 \times 10^{-2} Q_1 I_c + 3.60 I_c^2 R_{tc} \quad (kJ/h) \tag{28}$$

5.2.4.2. Heat balance during discharge. Similarly, discharge heat balance per unit time (Q_d) is expressed with Eq. (29).

$$Q_d = Q_r + Q_{pd} + Q_J = 3.73 \times 10^{-2} Q_1 I_d + 3.60 I_d^2 R_{pd} + 3.60 I_d^2 R_{ed} = 3.73 \times 10^{-2} Q_1 I_d + 3.60 I_d^2 R_{td} \quad (kJ/h) \tag{29}$$

5.2.5. Changes in reaction heat and Joule heat according to current value

Here, Eqs. (28) and (29) are used to analyze changes in reaction heat and Joule heat according to current value. In Eq. (28), the first term is the endothermic reaction heat; the second term, exothermic Joule heat. The first term in Eq. (29) is the exothermic reaction heat. This relationship is shown in Fig. 8.

The generated heat (Q_1) and internal resistance (R_t) contained in the first and second terms change depending

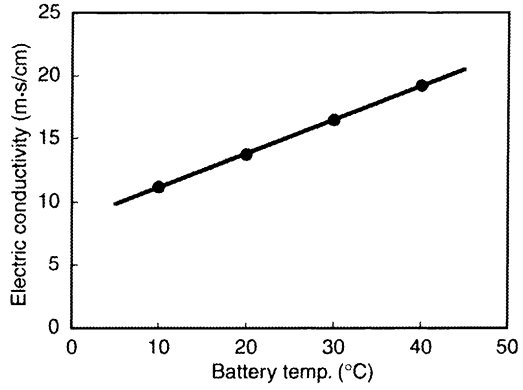

Fig. 7. Battery temperature dependence on electric conductivity of 1.0 M PC/DMC/$LiPF_6$ electrolyte.

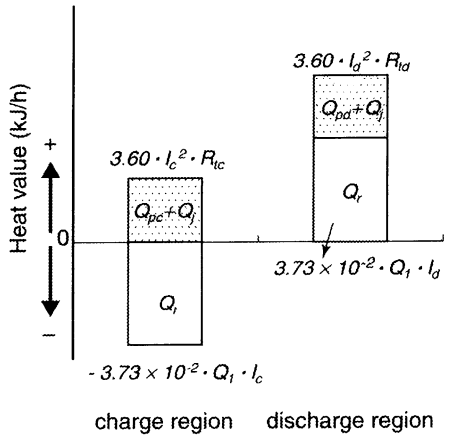

Fig. 8. Heat intake and release model of Li-ion batteries during charge and discharge process.

on DOD. Here, each term's heat generation is calculated for 50% DOD, a representative value. Q_1 is 9.39 kJ/mol while internal resistance (R_t) depends on battery size: 1–2 mΩ per EV cell, 3–5 mΩ per HEV cell. As these are test calculations, changes in the reaction heat and endothermic Joule heat during discharge were calculated with a value of 1.2 mΩ for 80 Ah EV cells and 4 mΩ for 3 Ah HEV cells (Fig. 9).

During charge, the heat of reaction is endothermic. In the case of the Li-ion battery for EV, the endothermic heat of reaction exceeds the exothermic Joule heat up to 70 or 80 A. Thus, Q_c, the value of heat during charge, is negative, and the battery temperature drops. During discharge, however, both the heat of reaction and Joule heat are exothermic, and the temperature rises continuously. In a Li-ion battery, the temperature increase due to the reaction heat makes a large contribution to total temperature increase up to 70 or 80 A, but beyond that, the contribution of Joule heat is larger.

In contrast, a low-capacity Li-ion battery, such as one designed for HEVs, has a larger internal resistance than a

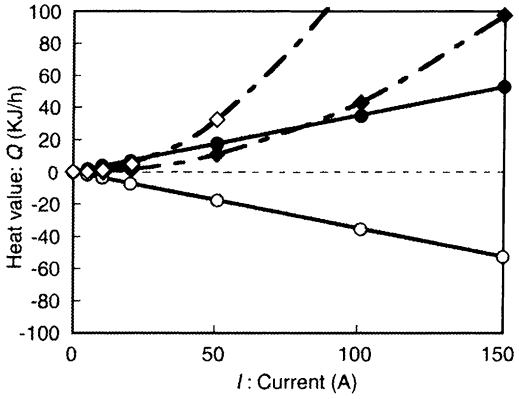

Fig. 9. Relationship between current and heat value. (●) Reaction heat value at discharge process of Li-ion batteries; (○) reaction heat value at charge process of Li-ion batteries; (◆) Joule heat value of 80 Ah prismatic Li-ion batteries for EV; (◇) Joule heat value of 3 Ah cylindrical Li-ion batteries for HEV.

Li-ion battery for EV, and so the contribution of exothermic Joule heat exceeds that of the reaction heat at about 20–30 A. In short, a Li-ion battery for HEV has a greater frequency occurrence of large currents of 20 A or higher, and so internal resistance must be reduced in order to prolong battery longevity.

6. Comparison of simulation and actual measurements

This section compares actual measurements with the results of heat generation simulation performed using Eqs. (28) and (29). From battery output (W) in the vehicle driving mode in Fig. 10, mode current value was calculated with Eq. (30), after which heat generation was calculated with Eq. (28) for negative current values. Eq. (29) was used for positive current values. Here, E_e was obtained from the relation between cell voltage and DOD, then 1.2 mΩ for 80 Ah EV cell was applied for R_t.

$$I = \frac{\{E_e - (E_e^2 - 4R_tW)^{1/2}\}}{2R_t} \quad (30)$$

As in Eq. (31), this heat generation value was divided by C (kJ/K) (battery heat capacity) to arrive at ΔT, battery temperature change per unit time. In accordance with the battery component materials, a value of 3.42 (kJ/K) was used for battery heat capacity. As Fig. 11 shows, the accuracy of simulation was improved by also including thermal radiation rate per unit time (T_r) at 25°C in an insulated state.

$$\Delta T = \frac{Q_t}{C} - T_r \ \text{(K/h)} \quad (31)$$

The results of simulation are shown in Fig. 12 along with the actual measurements. The actual measurements which were taken with a large 80 Ah Li-ion battery for EV wrapped in insulating material and so indicate a battery temperature in a state approaching an insulated one correspond well with the results of simulation. The reason for the slight discrepancy between the simulation results and actual measurements starting at 70% DOD is that the value of internal resistance R_t at 50% DOD was used throughout the simulation process for the purpose of simplification.

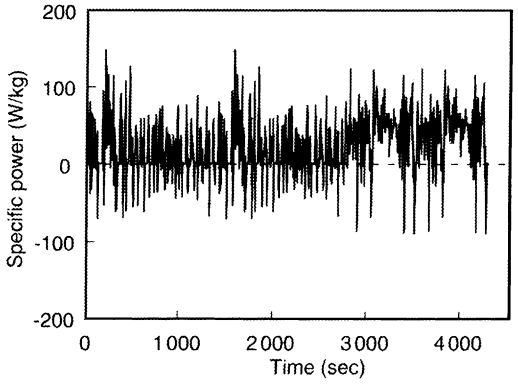

Fig. 10. Vehicle test mode.

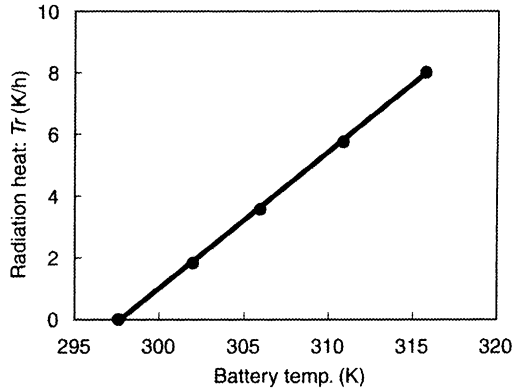

Fig. 11. Correlation between battery temperature and radiation heat with an adiabatic state.

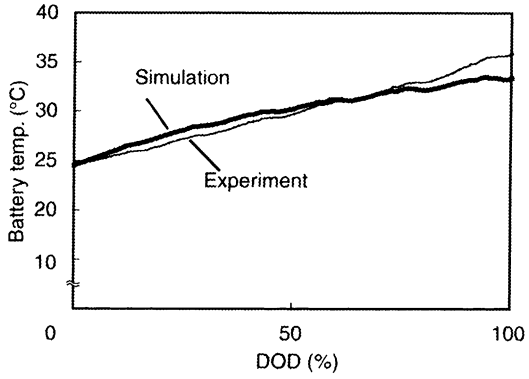

Fig. 12. Comparison of measured heat value with simulation data.

In actuality, internal resistance varies depending on DOD, showing a particularly large increase in the high DOD zone (Fig. 6). In other words, the simulated values were slightly larger than the measured values in the high DOD zone because the internal resistance value used in the simulation was lower than actual internal resistance.

The preceding verifies the theoretical correctness of the results of exothermic behavior analysis described in Section 5. Although the simulation described in this paper assumed a Li-ion battery for EV applications, similar trial calculations are, of course, also possible for HEV applications, as well.

7. Conclusion

Thermodynamic analysis of battery reactions permitted the fine categorization of the specific heat generation factors listed below, and the estimation of a battery's exothermic properties.

1. Heat generation factors can be divided into three types: reaction heat (Q_r), polarization heat (Q_p), and Joule heat

(Q_J), expressible as $Q_r = 3.73 \times 10^{-2} Q_1 I$, $Q_p = 3.60 R_p I^2$, and $Q_J = 3.60 R_e I^2$.

2. When used as the positive electrode, $LiCoO_2$ results in an endothermic reaction heat value during charge. In a large, 80 Ah Li-ion battery for EV, this endothermic reaction heat exceeds the exothermic Joule heat with a current value of up to 70 or 80 A, resulting in a negative value for charge heat (Q_c).
3. Further categorizing the heat generation factors into charge and discharge factors and performing simulation using these values yield results that corresponded well with actual measurements, thereby verifying the correctness of this analytic method.

8. Notes

The author's analysis of exothermic behavior mechanism not only made it possible to quantitatively analyze heat generation by a Li-ion battery under actual load conditions, but also provided guidelines for the design of Li-ion batteries for electric and hybrid vehicles. It is hoped that this paper will help further efforts to develop batteries for HEV and EV applications.

References

[1] Y. Saito, K. Kanari, K. Takano, T. Masuda, Battery Technol. 8 (1996) 129 (in Japanese).
[2] S. Al Hallaj, J. Prakash, J.R. Selman, J. Power Sources 87 (2000) 186.
[3] N. Sato, K. Yagi, Honda R&D Tech. Rev. 10 (1998) 32 (in Japanese).
[4] Z. Takehara (Ed.), High density lithium secondary battery — reaction and material development, Technosystem (1998) 45 (in Japanese).
[5] O. Chusid, Y. Ein-Eli, D. Aurbach, M. Babai, Y. Carmeli, J. Power Sources 43 (1993) 47.
[6] D. Aurbach, Y. Ein-Eli, O. Chusid, Y. Carmeli, M. Babai, H. Yamin, J. Electrochem. Soc. 141 (1994) 603.
[7] Y. Ein-Eli, B. Markovsky, D. Aurbach, Y. Carmeli, H. Yamin, S. Luski, Electrochem. Acta 39 (1994) 2559.
[8] D. Aurbach, Y. Ein-Eli, B. Markovsky, A. Zaban, S. Luski, Y. Carmeil, H. Yamin, J. Electrochem. Soc. 142 (1995) 2882.
[9] D. Aurbach, Y. Ein-Eli, J. Electrochem. Soc. 142 (1995) 1746.
[10] Y. Ein-Eli, S. Thomas, R. Chadha, T. Blakley, V. Koch, J. Electrochem. Soc. 144 (1997) 823.
[11] M. Yoshio, A. Kozawa, Material of lithium-ion secondary battery and applications, Nikkan Kogyo Shimbun (1996) 13 (in Japanese).